Materials Horizons

COMMUNICATION

Single crystal field-effect transistors of a highly dipolar merocyanine dye†

A. Liess, M. Stolte, T. He and F. Würthner*

The charge transport properties of a highly dipolar merocyanine dye are investigated in single crystal field-effect transistors. The devices reach a p-type mobility value of up to 2.34 cm^2 V^{-1} s^{-1} and calculations show that the charge transport mainly occurs along the π-stacking direction of the needle-like single crystals.

Conceptual insights

Dipolarity is so far considered as a disadvantageous property for charge carrier transport in organic solids. For amorphous semiconducting films a significant drop of performance has indeed been experimentally verified and theoretically explained by a broadening of the density of states. Accordingly, only few organic small molecules with a dipole moment have been used in organic electronics applications. Mainly driven by the fact that dipolar dyes tend to arrange in ordered dimer structures due to their dipolarity as well as good performance of dipolar dyes in organic solar cells, we started to conduct research on field-effect transistors of highly dipolar merocyanine dyes. In this study we show the first examples of single crystal field-effect transistor (SCFET) devices based on organic semiconductor molecules that exhibit a dipole moment (dipole moment of 13.3 D). SCFETs are undoubtedly the ideal choice to reveal the intrinsic conductivity properties of a material. Our results with p-type mobility values up to 2.34 cm^2 V^{-1} s^{-1} clearly indicate that high dipolarity is not necessarily disadvantageous but can lead also to devices with high mobility values, competing with values of conventional organic semiconductors.

Universität Würzburg, Institut für Organische Chemie & Center for Nanosystems Chemistry, Am Hubland, 97074 Würzburg, Germany.
* E-mail: wuerthner@chemie.uni-wuerzburg.de

1. Introduction

Organic semiconductor research enjoys already a long and very successful history.[1] Archetype classes of materials are polycyclic aromatic compounds, conjugated oligomers and polymers, and triarylamines and structurally related spiro compounds. Interestingly, these compounds take advantage of different materials properties which are of relevance for their respective utilization. Thus, triarylamines and related spiro compounds are among the best molecules for amorphous photoconductor materials for electrophotography due to their low reorganization energies for hole transfer and easy design of high temperature amorphous solids.[2] On the other hand, conjugated oligomers and polymers provide the currently leading p-semiconductor compounds for bulk heterojunction solar cells due to successful tunability of absorption and redox properties in combinations with n-semiconducting fullerene derivatives.[3] Finally, for organic transistors, highly crystalline small molecules such as pentacene and related heteroatom bearing compounds continue to prevail as the most promising materials.[4] In particular thienoacenes which combine structural motifs of acenes with another archetype class of organic semiconductors, i.e. oligothiophenes,[5] constitute nowadays the benchmark in the field with hole mobilities up to 43 cm^2 V^{-1} s^{-1}.[6] This raises the question if still better materials can be expected by newly developed molecules within the given structural space for instance by computational support[7] and a more in-depth understanding of charge carrier transport processes in organic solids where the debate about hopping versus band transport is still an ongoing one.[8]

Some years ago we suggested a different concept for high performance organic semiconductor molecules based on highly dipolar donor-acceptor (D–A) merocyanine dyes,[9] which have already been successfully used for photorefractive and nonlinear optics applications.[10] While the alternating sequence of donor and acceptor units is widely used in the field of polymer semiconductors to obtain ambipolar devices,[11] small molecules with high dipolarity are undoubtedly very

COMMUNICATION

Materials Horizons

problematic in amorphous state due to the impact of dipolar disorder on charge carrier transport[12] and accordingly delivered only low quality transistors in an initial study by Kudo *et al.*[13] However, their strong tendency to assemble in antiparallel dimers has been recognized by us and others already a while ago.[14] The pronounced electrostatic cohesive forces between highly dipolar dye molecules suggest that solid state materials might be obtained with more closely stacked dyes, higher density, higher refractive index, and increased charge transfer integrals between neighboring molecules compared to other π-conjugated molecules that are attracted merely by dispersion forces.

Interestingly, different from what might have been expected based on the previous analyses, very well performing amorphous materials could be obtained from dipolar merocyanine dyes in bulk heterojunction solar cells (power conversion efficiencies exceeding 6%)[15] and even organic thin-film transistors (OTFTs) exhibiting moderate mobilities (0.05 $cm^2 V^{-1} s^{-1}$) were fabricated from a dipolar hexacene derivative.[16] This shows that the formation of centrosymmetrically stacked dimers or even more regular structures is sufficient to narrow the energy dispersion by dipolar disorder. On the other hand, with our highly dipolar mecocyanine dyes, realization of high performance OTFTs proved to be difficult because the vast majority of the dyes did not grow in crystalline layers on various substrates while thin films of some dyes showed promising charge transport behavior (0.18 $cm^2 V^{-1} s^{-1}$).[17,18] This brought us to consider single crystal field-effect transistors (SCFETs)[19] which open up the chance to shed light into the fundamental scopes and limitations for charge carrier transport in organic solid state materials (for a schematic description, see Fig. 1a). As SCFETs by their definition lack grain boundaries but show a perfect molecular order, they are the ideal tool to investigate the

intrinsic charge carrier transport properties. Thus, herein we report the first application of a highly dipolar merocyanine dye as organic semiconductor in SCFETs and show a maximum mobility of 2.34 $cm^2 V^{-1} s^{-1}$.

Notably, this value is more than one order of magnitude higher than the value obtained for OTFTs for this dye (0.13 $cm^2 V^{-1} s^{-1}$) as well as higher than the value for OTFTs of another merocyanine dye (0.64 $cm^2 V^{-1} s^{-1}$)[20] which so far constituted the benchmark for dipolar organic semiconductors.

2. Experimental Section

Synthesis and Materials: The synthesis of our merocyanine dye **1**, whose molecular structure consists of a D–A structure with 1-butyl-3,3-dimethylindolin-2-ylidene ('Fischer base') as donor and 2-(4-alkylthiazol-2(3H)-ylidene)malononitrile as acceptor unit has been described previously.[21] The *n*-tetradecylphosphonic acid (TPA) modified substrates were prepared by atomic layer deposition of a 8 nm thick AlO_x layer onto boron doped p-type Si(100) wafers with 100 nm SiO_2 as dielectric and subsequent immersion of the $Si/SiO_2/AlO_x$ substrates into isopropanol solutions of TPA. With this method, 1.7 nm thick monolayers of TPA were obtained (capacitance of the whole dielectric C_i = 32.4 nF cm^{-2}). As solvents, $CHCl_3$ (≥99 %, anhydrous grade) and MeOH (p.a. grade) were used.

Device Fabrication: Single crystal field-effect transistors of merocyanine dye **1** were fabricated according to a previously described method[22] as follows (for a schematic description, see Fig. S1, ESI†). A saturated solution of dye **1** in $CHCl_3$ (c = 7.0·10^{-3} M, filtered with a 0.2 µm PTFE syringe filter) was
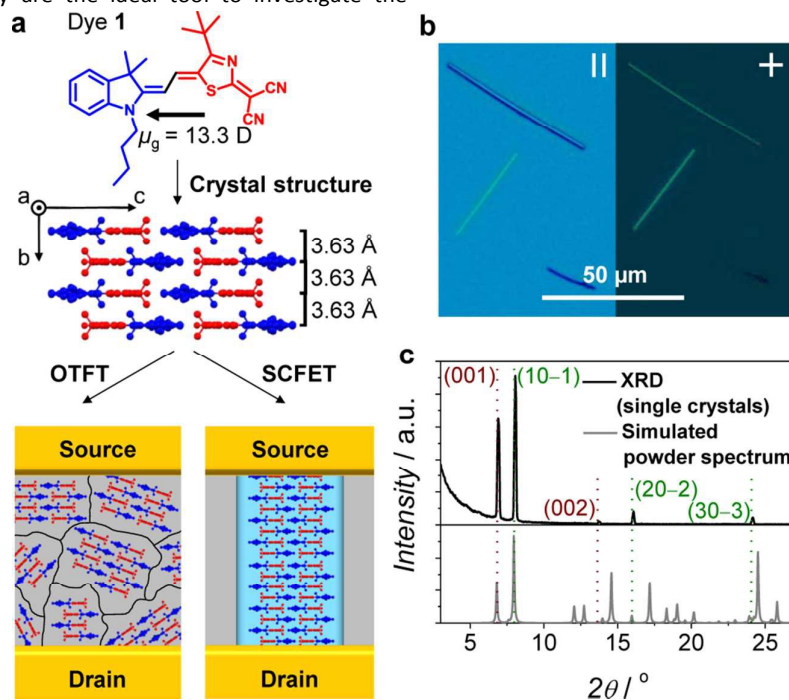
Fig. 1 (a) Molecular structure of merocyanine dye **1** together with packing in the single crystal with view along the *a*-axis and schematic top views on OTFTs[17] and SCFETs (this work) with respective molecular ordering. The donor parts of the molecules are colored in blue, the acceptor parts in red and hydrogens are omitted for clarity in the single crystal structure. (b) Bright-field microscopy image and cross-polarized microscopy image of single crystals of merocyanine dye **1** on TPA modified $Si/SiO_2/AlO_x$ substrate. (c) XRD pattern of single crystals of merocyanine dye **1** on TPA modified $Si/SiO_2/AlO_x$ substrate (black line) in comparison with a powder pattern simulated from the single crystal structure (grey line) and indexed reflexes arising from two sets of lattice planes (red and green lines).

prepared and then mixed with MeOH to give solutions of volumetric mixing ratios 3:2 or 2:1. A TPA modified Si/SiO$_2$/AlO$_x$ substrate was placed onto a PTFE plate inside a sealable container (50 mm in diameter, 30 mm in height), together with two screw caps which were filled with 250 µl of a CHCl$_3$:MeOH mixture (volume ratio 1:1). A small piece of PTFE was placed in the middle of the substrate and the container was closed and heated to 30 °C for 1 h to saturate the container with an atmosphere of the mixed solvents. Then, the substrate was wetted by the prepared solution and the container was closed and sealed with parafilm. After 3 d, the solvent in the screw caps and on the substrate was completely evaporated and single crystals were obtained. Next, the substrates were heated for 1 h to 40 °C in vacuum to remove residual solvent and 100 nm gold were deposited onto the single crystals with a gold wire of either 25 µm or 12.7 µm as shadow mask to yield source and drain electrodes. Thermal evaporation of the gold was done with a rate of 0.03 nm s^{-1} - 0.05 nm s^{-1} and a pressure below $3 \cdot 10^{-6}$ mbar.

Device Characterization: All SCFETs were electrically characterized by measuring transistor current voltage characteristics with a Micromanipulator 4060 and an Agilent 4155C semiconductor parametric analyzer (Agilent Technologies, Inc. Santa Clara, CA) at ambient conditions. Beforehand, the devices were electrically isolated by scratching the surrounding of the single crystal with a needle of the micromanipulator. Atomic force microscopy was done in tapping mode with a NT-MDT SOLVER NEXT instrument and silicon cantilevers (OMCL-AC160TS, Olympus) with a spring constant of 42 N m^{-1}. X-ray diffraction experiments were carried out with a Bruker D8 Discover diffractometer with a LynxEye-1D-Detector using Cu K$_\alpha$ radiation (K$_{\alpha 1}$ + K$_{\alpha 2}$ doublet, mean wavelength λ = 154.19 pm). Scanning electron microscopy was performed using a Zeiss Ultra Plus FE-SEM equipped with a GEMINI e-Beam column operated at 3 - 5 kV. The images with ESB detector were obtained with a grid voltage of 530 V. Transmission electron microscopy and selected area electron diffraction (SAED) measurements were done with a FEI Titan 80-300 transmission electron microscope at an accelerating voltage of 150 kV. Nanocrystals of dye **1** were grown on a copper grid covered with carbon as described above. In this case however, no small PTFE piece was placed in the middle of the copper grid as the grid was too small.

Calculations: The BFDH morphology was calculated from the single crystal structure with the program Mercury.[23] Calculations of the transfer integrals were done by a fragment orbital approach[24] and a basis set orthogonalization procedure[25] with the ADF (Amsterdam density functional) package[26] using the B3LYP functional[27] and TZP basis set.

3. Results and discussion

In order to fabricate SCFETs, crystals of dye **1** were firstly grown from a CHCl$_3$/MeOH solution on *n*-tetradecylphosphonic acid (TPA) modified Si/SiO$_2$/AlO$_x$ wafers. These crystals exhibited needle-like shapes with varying lengths from several micrometers up to hundreds of micrometers (see Fig. S2 - S7, ESI†). Our earlier work showed that this dye crystallizes in a brickwork-type pattern where the molecules are aligned antiparallel, mainly driven by their ground state dipole moment of 13.3 D.[17] To verify the crystalline structure of the single crystals on the substrate, out-of-plane X-ray diffraction (XRD) experiments were carried out. In the obtained diffraction pattern, five diffraction peaks at 2θ = 6.9°, 8.1°, 13.7°, 16.1° and 24.1° could be observed (see Fig. 1c). Compared to a powder spectrum, which was simulated based on the single crystal structure with the program Mercury,[23] these peaks could be identified as resulting from two sets of lattice planes: (001) and (002), as well as (10–1), (20–2) and (30–3). Hence, with this fabrication, two different orientations of single crystals are obtained on the TPA modified wafers which might have an impact on the transistor behavior as the charge injection from two differently aligned metal/organic interfaces could vary as it is discussed later.[28] To ensure crystallinity, selected area electron diffraction (SAED) measurements were performed additionally (see Fig. S8, ESI†). In these experiments, a clear diffraction pattern was observed which confirms that these needles are indeed single crystals. The diffraction pattern along the elongation direction of the needle gives a lattice spacing of 7.3 Å which coincides well with the single crystal lattice parameter b = 7.2565 Å and thus demonstrates that the needles are elongated along the b-axis which is also the π-π-stacking direction.

Next, homogeneous crystals with thicknesses d smaller than 1.0 µm were selected and 100 nm thick gold source and drain electrodes were deposited in vacuum according to the gold wire shadow mask technique (Fig. S1, ESI†).[29] Finally, the transfer and output characteristics of the devices were measured under ambient conditions with a drain-source voltage of V_{DS} = −50 V in the saturation regime. Estimation of the charge carrier mobility μ was carried out according to the equation $\mu = (2I_{DS}L/[WC_i(V_{GS}-V_T)^2])$, where I_{DS} denotes the drain-source current, V_{GS} the gate-source voltage, V_T the threshold voltage and L and W describe the transistor channel length and width, respectively. The capacitance per area of the dielectric C_i was 32.4 nF cm^{-1}.
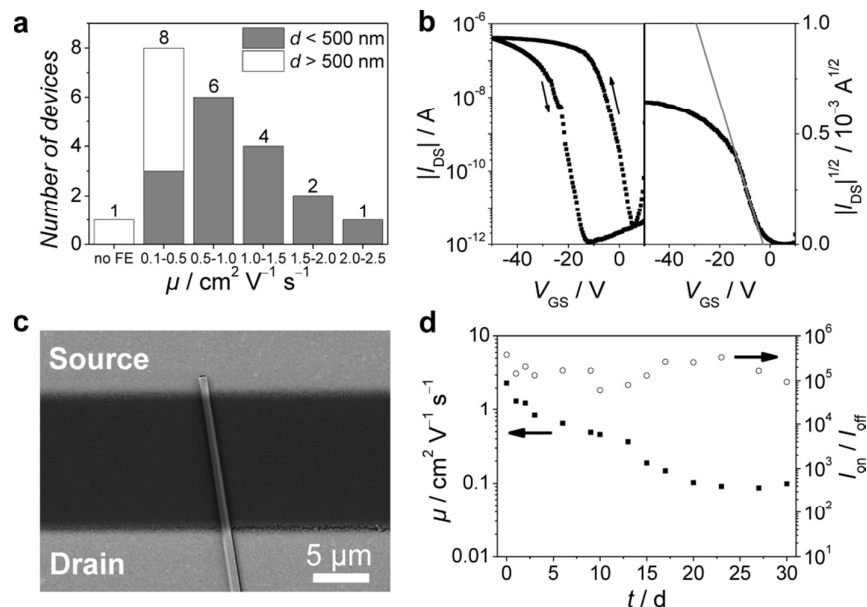
Fig. 2 (a) Distribution of the mobility values of all 22 devices. (b) Transfer curve of representative device (left) with plot of the square root of the drain-source current (right) and corresponding linear fit (grey line). (c) SEM picture of representative device. (d) Development of the mobility (filled squares) and on/off ratio (open circles) of representative device over 30 d when kept in air.

In total, 22 SCFETs were fabricated, out of which only one device did not work. A graphic illustration of the mobility distribution of all SCFETs is shown in Fig. 2a while their transfer curves, device dimensions and SCFET parameters are provided in the ESI†, Fig. S2 – S7, Fig. S9 and Tab. S1. The transfer curve as well as a SEM image of a representative device are depicted in Fig. 2b,c. Note, that the plot of $(I_{DS})^{1/2}$ vs. V_{GS} shows a nonlinear behavior giving rise to only a narrow V_{GS} region where optimal performance is given. This non-ideality cannot be attributed to contact resistance as no S-shape in the linear regime as well as no drop of I_{DS} in the saturation regime can be observed in the output curve (Fig. S10a, ESI†). Despite this obvious drawback, which might originate from fabrication and characterization in ambient media, we will deduce in the following all mobilities in this region of optimal operation to demonstrate the propensity of merocyanine dyes in SCFETs.

All devices showed p-type field-effect mobilities ranging from 0.11 cm^2 V^{-1} s^{-1} up to 2.34 cm^2 V^{-1} s^{-1}, yielding an average device mobility of 0.87 cm^2 V^{-1} s^{-1}, while the threshold voltages of the devices varied from −13 V to 0 V and the on/off ratios were determined to be in the range of 10^3 - 10^5. As it is known that the thickness of single crystals in bottom gate top contact transistor devices can play a crucial role in terms of device performance – an increasing crystal thickness will lead to a limited drain-source current due to an increasing contact resistance[30] – the thicknesses of the nano crystals have been investigated by atomic force microscopy (AFM) and show a

wide variety with values from 49 nm to 930 nm. For devices with thicknesses $d < 500$ nm, the average mobility rises to 1.05 cm^2 V^{-1} s^{-1} while the range of the threshold voltage and the on/off ratio does not change compared to the crystals with higher thicknesses.

Investigations on the device stability was performed on the best SCFET (Fig. 2b) with a mobility of 2.34 cm^2 V^{-1} s^{-1}, a threshold voltage of −3 V and an on/off ratio of 4·10^5. Keeping the device in air for 45 d shows a decrease of the mobility to below 10% of its initial value after 20 d while then staying constant (Fig. 2d). When tested again after 45 d, the device showed no transistor behavior anymore and a recovery of device performance by annealing in vacuum was not possible during the degradation process (see Fig. S10b, ESI†). As the on-current decreases in almost the same manner as the mobility, the decrease of the mobility can be explained by a reduction of the on-current which shows a similar time-dependent course (Fig. S10c, ESI†). However, in terms of threshold voltage and on/off ratio, the device shows a good stability. Over 30 d, the threshold voltage shows only a small shift from −3 V to −6 V while the on/off ratio remains almost constant and drops only from 4·10^5 to 9·10^4 (see Fig. 2d and Fig. S10c, ESI†). Storage of the devices in different environments, i.e. argon, ambient, dry and humid air (100 % relative humidity), showed no improvement of the device stability (see Fig. S11, ESI†). Thus we attribute the device degradation to the fabrication and the characterization under ambient conditions.
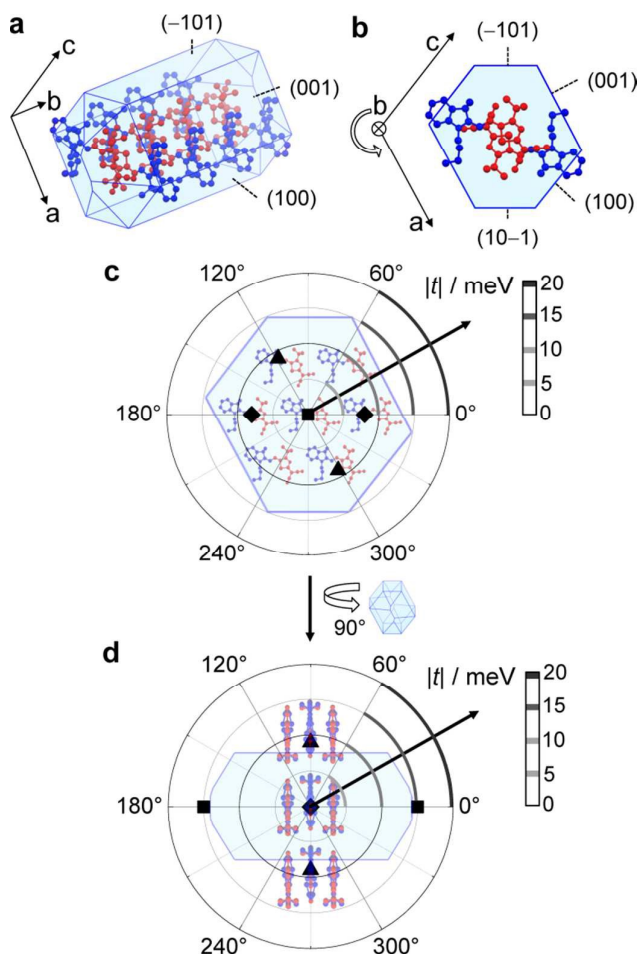
Fig. 3 (a) BFDH morphology of a single crystal of dye **1** with crystallographic direction and indexed relevant lattice planes. (b) View on the (010) plane of the BFDH morphology with indexed relevant lattice planes as well as possible rotation direction around the *b*-axis of the elongated crystals. (c) Calculated transfer integrals *t* for next neighboring molecules with view on the (010) plane as well as (d) for next neighboring molecules with view along the [101] direction.

It should be noted that the transfer curves of the devices show a hysteresis for which the drain-source current is higher for the forward than for the backward measurement cycle. The hysteresis broadens for measurements at higher temperatures and for measurements with a lower sweep rate (Fig. S12, ESI†). This behavior suggests a slow response of mobile charge carriers to the applied electrical field,[31] for which a polaronic/bipolaronic mechanism is proposed in the filed of conjugated polymers.[31,32] Whether this mechanism applies for the devices of merocyanine dye **1** in air is however beyond the scope of this communication. Either way, the hysteresis can be significantly reduced if the gate-source voltage is swept only up to −30 V (see Fig. S13, ESI†) which shows that the devices suffer from electrical stress when the gate-source voltage is swept up to −50 V.

To gain insight into the intrinsic charge carrier transport properties, the Bravais-Friedel-Donnay-Harker (BFDH) morphology of the crystals was calculated from the single crystal structure with the program Mercury[23] (see Fig. 3a,b).

The calculation demonstrates a needle-like morphology in accordance to the experimental observation with an elongation along the *b*-axis which is equal to the π-π-stacking direction of the molecules. Furthermore, it can be easily rationalized why two different orientations (001) and (10−1) of the crystal planes can be observed by XRD experiments (see Fig. 1c), as they result from a simple rotation around the *b*-axis of the elongated crystals (see Fig. 3b). This lack of preferential out-of-plane orientation corresponds to the fact that the TPA modified surface has a low surface energy[33] which might result in a low interaction of the surface with the organic molecules.

DFT calculations of the transfer integrals *t* for the next neighbors of a molecule showed that hole transport is in fact possible in three directions, namely the [010] (*b*-axis), the [101] and the [100] directions (see Fig. 3c,d). The calculations elucidated that for all of these three directions, the transfer integral has similar values of 8 meV (direction [101]), 9 meV (direction [100]) and 15 meV (direction [010]), while for next neighbors in other directions the calculations of the transfer integrals resulted in a value of zero (see Fig. S14 and Tab. S2, ESI†). These results suggest that for an applied electrical field in the [010] direction, i.e. along the drain-source channel of the SCFETs, the charge carriers will be transported mainly along the π-π-stacking direction. The injection of the charge carriers, however, should mainly take place within the (010) plane as this stands upright on the surface. As a two dimensional charge transport within this plane is possible with almost equal transfer integrals for two directions [101] and [100], the orientation of the crystal on the substrate actually makes no difference for charge injection. Furthermore, these results with similar transfer integrals in three linearly independent directions show that even with traps or defects present in the channel region, a charge carrier can easily circumvent these and be transported within the brickwork-type packing arrangement of the dyes.

4. Conclusions

In conclusion, needle-like single crystals of the highly dipolar merocyanine dye **1** were grown on TPA modified Si/SiO$_2$/AlO$_x$ substrates from solution under ambient conditions. With vacuum deposition of gold source and drain electrodes, SCFETs were fabricated which for devices with thicknesses *d* < 500 nm showed an average mobility of 1.05 cm^2 V^{-1} s^{-1} with the best device reaching a value of 2.34 cm^2 V^{-1} s^{-1} measured in air. This value is indeed comparable to those found for SCFETs of typical p-type organic semiconductors such as tetracene (2.4 cm^2 V^{-1} s^{-1}),[34] TIPS-pentacene (5.0 cm^2 V^{-1} s^{-1})[35] and copper phthalocyanine (1.0 cm^2 V^{-1} s^{-1}).[36] Only for very few other molecules, i.e. DNTT (9.9 cm^2 V^{-1} s^{-1}),[37] pentacene (40 cm^2 V^{-1} s^{-1})[38] and rubrene (40 cm^2 V^{-1} s^{-1}),[39] higher values could be observed. It is also noteworthy that the devices of molecules showing higher mobilities were prepared either in a clean room in the case of rubrene or measured under inert conditions (DNTT and pentacene), while both the fabrication and characterization of the devices of our merocyanine dye **1** were carried out under ambient conditions. Thus, this is the first time that high mobility values >1.00 cm^2 V^{-1} s^{-1} are

demonstrated for organic field-effect transistor devices consisting of a highly dipolar compound (dipole moment of 13.3 D) as organic semiconductor. Therefore, high dipolarity should not be considered disadvantageous for crystalline organic semiconductors. Because the π-π-distance of merocyanine dye **1** is quite high with 3.63 Å, dipolar D–A compounds with lower π-π-distances are expected to afford even higher mobility values in transistor devices.

Acknowledgements

Notes and references

1   M. Schwoerer and H. C. Wolf, *Organic Molecular Solids*, Wiley-VCH, Weinheim, Germany, 2007.
2   (*a*) Y. Shirota, *J. Mater. Chem.*, 2000, **10**, 1; (*b*) D. S. Weiss and M. Abkowitz, *Chem. Rev.*, 2010, **110**, 479.
3   (*a*) P.-L. T. Boudreault, A. Najari and M. Leclerc, *Chem. Mater.*, 2011, **23**, 456; (*b*) L. Dou, J. You, Z. Hong, Z. Xu, G. Li, R. A. Street and Y. Yang, *Adv. Mater.*, 2013, **25**, 6642.
4   (*a*) J. E. Anthony, *Angew. Chem. Int. Ed.*, 2008, **47**, 452; (*b*) J. Mei, Y. Diao, A. L. Appleton, L. Fang and Z. Bao, *J. Am. Chem. Soc.*, 2013, **135**, 6724.
5   A. Mishra, C.-Q. Ma and P. Bäuerle, *Chem. Rev.*, 2009, **109**, 1141.
6   (*a*) K. Takimiya, S. Shinamura, I. Osaka and E. Miyazaki, *Adv. Mater.*, 2011, **23**, 4347; (*b*) Y. Yuan, G. Giri, A. L. Ayzner, A. P. Zoombelt, S. C. B. Mannsfeld, J. Chen, D. Nordlund, M. F. Toney, J. Huang and Z. Bao, *Nat. Commun.*, 2014, **5**, 3005.
7   V. Coropceanu, J. Cornil, D. A. da Silva Filho, Y. Olivier, R. Silbey and J.-L. Brédas, *Chem. Rev.*, 2007, **107**, 926.
8   S. Mehraeen, V. Coropceanu and J.-L. Brédas, *Phys. Rev. B*, 2013, **87**, 195209.
9   F. Würthner and K. Meerholz, *Chem. Eur. J.*, 2010, **16**, 9366.
10 (*a*) L. Beverina and G. A. Pagani, *Acc. Chem. Res.*, 2014, **47**, 319; (*b*) S. R. Marder, B. Kippelen, A. K.-Y. Jen and N. Peyghambarian, *Nature*, 1997, **388**, 845; (*c*) F. Würthner, R. Wortmann, R. Matschiner, K. Lukaszuk, K. Meerholz, Y. DeNardin, R. Bittner, C. Bräuchle and R. Sens, *Angew. Chem. Int. Ed. Engl.*, 1997, **36**, 2765; (*d*) C. B. Gorman and S. R. Marder, *Proc. Natl. Acad. Sci. U. S. A.*, 1993, **90**, 11297.
11 H. Usta, C. Newman, Z. Chen and A. Facchetti, *Adv. Mater.*, 2012, **24**, 3678.
12 (*a*) A. Dieckmann, H. Bässler and P. M. Borsenberger, *J. Chem. Phys.*, 1993, **99**, 8136; (*b*) D. Hertel and H. Bässler, *ChemPhysChem*, 2008, **9**, 666.
13 K. Kudo, M. Yamashina and T. Moriizumi, *Jpn. J. Appl. Phys.*, 1984, **23**, 130.
14 (*a*) L. R. Dalton, A. W. Harper and B. H. Robinson, *Proc. Natl. Acad. Sci. U. S. A.*, 1997, **94**, 4842; (*b*) F. Würthner and S. Yao, *Angew. Chem. Int. Ed.*, 2000, **39**, 1978.
15 (*a*) V. Steinmann, N. M. Kronenberg, M. R. Lenze, S. M. Graf, D. Hertel, K. Meerholz, H. Bürckstümmer, E. V. Tulyakova and F. Würthner, *Adv. Energy Mater.*, 2011, **1**, 888; (*b*) A. Arjona-Esteban, J. Krumrain, A. Liess, M. Stolte, L. Huang, D. Schmidt, V. Stepanenko, M. Gsänger, D. Hertel, K. Meerholz, F. Würthner, *J. Am. Chem. Soc.*, 2015, **137**, 13524; (*c*) for related work on other highly dipolar donor-acceptor dyes in organic photovoltaics, see E. Ripaud, T. Rousseau, P. Leriche and J. Roncali, *Adv. Energy Mater.*, 2011, **1**, 540; (*d*) H.-W. Lin, S.-W. Chiu, L.-Y. Lin, Z.-Y. Hung, Y.-H. Chen, F. Lin and K.-T. Wong, *Adv. Mater.*, 2012, **24**, 2269.
16 Q. Miao, M. Lefenfeld, T.-Q. Nguyen, T. Siegrist, C. Kloc and C. Nuckolls, *Adv. Mater.*, 2005, **17**, 407.
17 A. Liess, L. Huang, A. Arjona-Esteban, A. Lv, M. Gsänger, V. Stepanenko, M. Stolte and F. Würthner, *Adv. Funct. Mater.*, 2015, **25**, 44.
18 L. Huang, M. Stolte, H. Bürckstümmer and F. Würthner, *Adv. Mater.*, 2012, **24**, 5750.
19 (*a*) L. Jiang, H. Dong and W. Hu, *J. Mater. Chem.*, 2010, **20**, 4994; (*b*) M. Wang, J. Li, G. Zhao, Q. Wu, Y. Huang, W. Hu, X. Gao, H. Li and D. Zhu, *Adv. Mater.*, 2013, **25**, 2229; (*c*) V. Podzorov, *MRS Bull.*, 2013, **38**, 15; (*d*) L. Shaw and Z. Bao, *Isr. J. Chem.*, 2014, **54**, 496.
20 A. Lv, M. Stolte and F. Würthner, *Angew. Chem. Int. Ed.*, 2015, **54**, 10512.
21 S. Krause, M. Stolte, F. Würthner and N. Koch, *J. Phys. Chem. C*, 2013, **117**, 19031.
22 T. He, M. Stolte and F. Würthner, *Adv. Mater.*, 2013, **25**, 6951.
23 C. F. Macrae, P. R. Edgington, P. McCabe, E. Pidcock, G. P. Shields, R. Taylor, M. Towler and J. van de Streek, *J. Appl. Crystallogr.*, 2006, **39**, 453.
24 K. Senthilkumar, F. C. Grozema, F. M. Bickelhaupt and L. D. A. Siebbeles, *J. Chem. Phys.*, 2003, **119**, 9809.
25 E. F. Valeev, V. Coropceanu, D. A. da Silva Filho, S. Salman and J.-L. Brédas, *J. Am. Chem. Soc.*, 2006, **128**, 9882.
26 ADF, 2013.01, Scientific Computing and Modelling NV, Amsterdam, 2013.
27 (*a*) A. D. Becke, *Phys. Rev. A*, 1988, **38**, 3098; (*b*) A. D. Becke, *J. Chem. Phys.*, 1993, **98**, 5648; (*c*) C. Lee, W. Yang and R. G. Parr, *Phys. Rev. B*, 1988, **37**, 785.
28 T. He, X. Zhang, J. Jia, Y. Li and X. Tao, *Adv. Mater.*, 2012, **24**, 2171.
29 Q. Tang, H. Li, M. He, W. Hu, C. Liu, K. Chen, C. Wang, Y. Liu and D. Zhu, *Adv. Mater.*, 2006, **18**, 65.
30 L. Jiang, W. Hu, Z. Wei, W. Xu and H. Meng, *Adv. Mater.*, 2009, **21**, 3649.
31 M. Egginger, S. Bauer, R. Schwödiauer, H. Neugebauer and N. S. Sariciftci, *Monatsh. Chem.*, 2009, **140**, 735.
32 (*a*) G. Paasch, S. Scheinert, A. Herasimovich, I. Hörselmann and T. Lindner, *Phys. Status Solidi A*, 2008, **205**, 534; (*b*) M. Qu, H. Li, R. Liu, S.-L. Zhang and Z.-J. Qiu, *Nat. Commun.*, 2014, **5**, 3185; (*c*) A. Salleo and R. A. Street, *Phys. Rev. B*, 2004, **70**, 235324; (*d*) R. A. Street, A. Salleo and M. L. Chabinyc, *Phys. Rev. B*, 2003, **68**, 085316.
33 S. Yogev, R. Matsubara, M. Nakamura, U. Zschieschang, H. Klauk and Y. Rosenwaks, *Phys. Rev. Lett.*, 2013, **110**, 036803.
34 C. Reese, W.-J. Chung, M.-M. Ling, M. Roberts and Z. Bao, *Appl. Phys. Lett.*, 2006, **89**, 202108.
35 G. Xue, C. Fan, J. Wu, S. Liu, Y. Liu, H. Chen, H. L. Xin and H. Li, *Mater. Horiz.*, 2015, **2**, 344.
36 R. Zeis, T. Siegrist and C. Kloc, *Appl. Phys. Lett.*, 2005, **86**, 022103.
37 W. Xie, K. Willa, Y. Wu, R. Häusermann, K. Takimiya, B. Batlogg and C. D. Frisbie, *Adv. Mater.*, 2013, **25**, 3478.
38 O. D. Jurchescu, M. Popinciuc, B. J. van Wees and T. T. M. Palstra, *Adv. Mater.*, 2007, **19**, 688.
39 J. Takeya, M. Yamagishi, Y. Tominari, R. Hirahara, Y. Nakazawa, T. Nishikawa, T. Kawase, T. Shimoda and S. Ogawa, *Appl. Phys. Lett.*, 2007, **90**, 102120.

Materials Horizons

TOC Entry
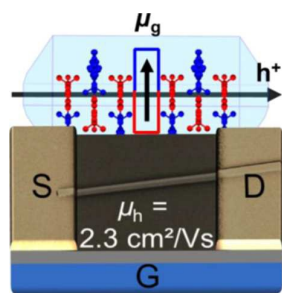
Single crystal field-effect transistors of a highly dipolar merocyanine dye reach p-type mobility values of up to 2.34 cm^2 V^{-1} s^{-1} in air.